

# The fabrication of superhydrophobic PTFE/UHMWPE composite surface by hot-pressing and texturing process

Wei Zhu<sup>1</sup> · Hongtao Liu<sup>1</sup> · Wei Yan<sup>1</sup> · Tianchi Chen<sup>2</sup>

Received: 20 July 2016 / Revised: 8 December 2016 / Accepted: 23 February 2017 / Published online: 9 March 2017  
© Springer-Verlag Berlin Heidelberg 2017

**Abstract** In this paper, we focus on improving the durability and repairability of superhydrophobic polytetrafluoroethylene (PTFE)/ultra-high-molecular-weight polyethylene (UHMWPE) composite coating via hot-press and followed texture treatment by weight and sandpaper. The hydrophobic properties were characterized by water contact angle measurement. A scanning electron microscope and step device were used to analyze the surface appearance. The anti-icing performance was characterized by a steam-freezing test in an environmental test chamber. The high-speed camera was used to analyze water droplet bouncing process and low adhesion property. The results show that the PTFE/UHMWPE superhydrophobic surface can be successfully fabricated by the hot-press and texture treatment with a contact angle of  $150 \pm 0.5^\circ$ . Both the anti-icing performance and low adhesion property show an excellent level. Moreover, the total energy just consumed about 30%, as the water droplet in the process of falling and contacting was at a 10 mm height.

**Keywords** Superhydrophobic · PTFE/UHMWPE polymer · Anti-icing · Low adhesion

## Introduction

Superhydrophobic surfaces were derived from the leaves and petals of various plants and body structures of several insets in nature, which possess contact angles higher than  $150^\circ$  and sliding angle lower than  $10^\circ$  [1]. In the recent decade, superhydrophobic surfaces have received urgent attention because of their remarkable significance in both fundamental research and potential industrial applications, including self-cleaning [2–4], transparent coatings [5–7], antifogging [8], anticorrosion [9–11], oil/water separation [12, 13], anti-icing [14, 15], and selective transportation of microdroplets [16–18]. On the basis of the results of previous studies, there are two methods to fabricate superhydrophobic surfaces: firstly, preparation of a hierarchical rough structure and then modification with low-energy materials and the other is creation of a hierarchical rough surface on low-energy materials directly [19, 20]. However, both surface structure and modification of low surface energy material are extremely fragile. Therefore, the excellent properties and available repairability are greatly important with respect to the wide application of superhydrophobic surfaces. However, until now, the superhydrophobic surface preparation of large-scale applications is still scarce due to the difficulty in the fragility of extreme conditions. To solve this dilemma, a few groups have attempted to fabricate superhydrophobic surfaces with outstanding durability and repairability. For example, Zhang et al. have obtained a superhydrophobic PEEK/polytetrafluoroethylene (PTFE) composite coating by changing the curing temperature on 45 steel substrates [21]. Cardoso et al. fabricated the hydrophobic polymer surfaces through laser micro structuring [22]. Although the excellent superhydrophobic surface can be created by aforementioned approaches, it can be repaired rarely. Huang et al. fabricated superhydrophobic heterostructure with self-repairing property via ultraviolet irradiation, but it is fragile [23].

✉ Hongtao Liu  
liuht100@126.com

<sup>1</sup> College of Materials Science and Engineering, China University of Mining and Technology, Xuzhou, Jiangsu 221116, China

<sup>2</sup> College of Mechanical & Electrical Engineering, China University of Mining and Technology, Xuzhou, Jiangsu 221116, China

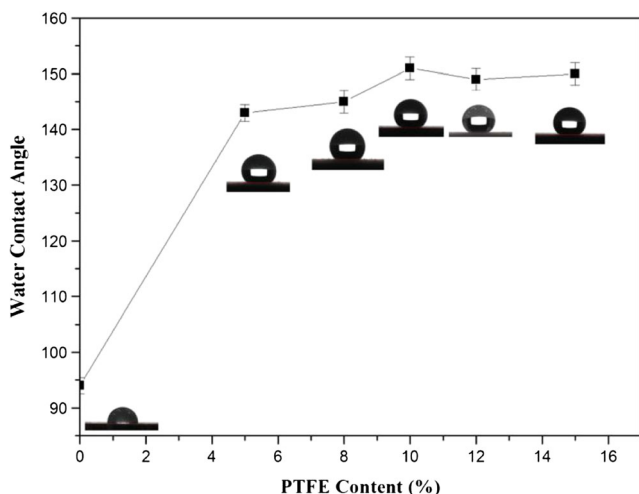


**Fig. 1** The contact angle values under different PTFE contents

Therefore, it is necessary to seek a facile and inexpensive method for fabricating both repairable and robust superhydrophobic surface.

Compared with other plastics, ultra-high-molecular-weight polyethylene (UHMWPE) is an extensively used thermoplastic engineering plastics due to its excellent properties, such as high strength and toughness, low friction coefficient, easy

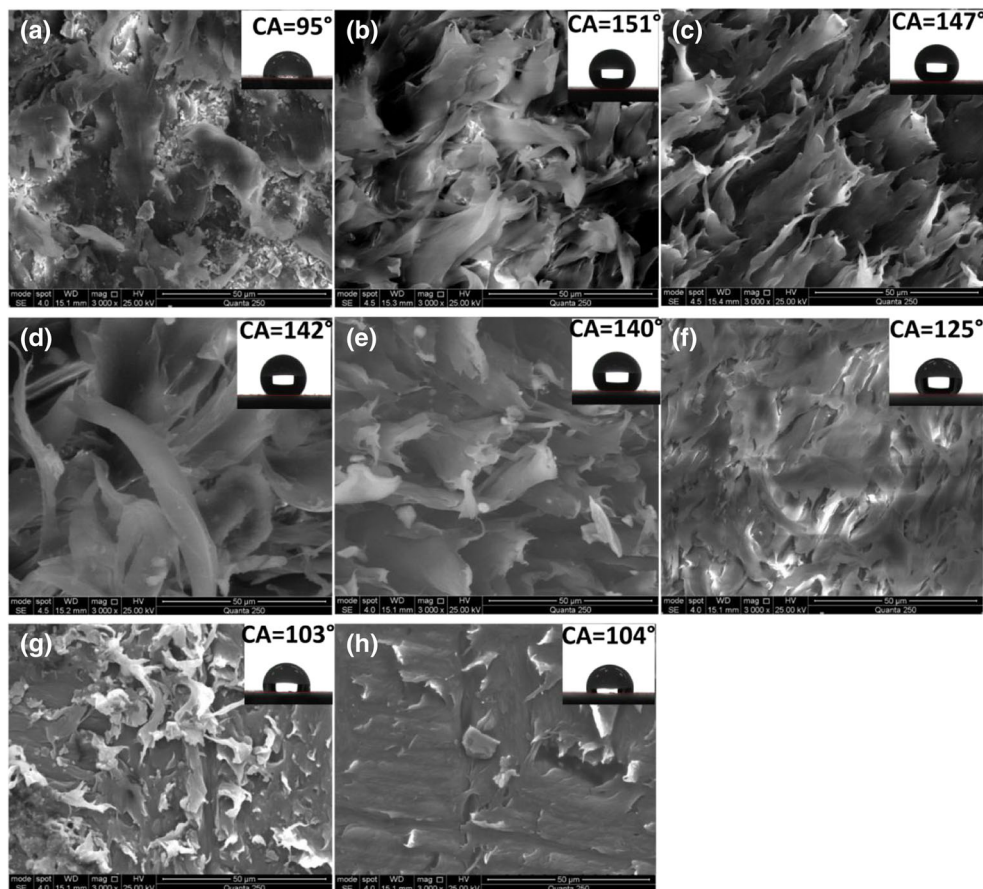
processing, and low cost [24, 25]. Additionally, the UHMWPE combined with nano-powder of PTFE has a great hydrophobic property compared to the pure UHMWPE. Herein, we provide a new method to fabricate superhydrophobic surface through texturing the PTFE/UHMWPE polymer. The influences of the PTFE concentration and the texture morphology on PTFE/UHMWPE superhydrophobicity were investigated. Furthermore, we discussed the superhydrophobic mechanism, anti-icing performance, and low adhesion of the prepared surface.

## Experimental

### Materials

UHMWPE powder (10–20  $\mu\text{m}$ ) and PTFE nano-particles (15–20 nm) were used as the matrix and additive of the composite, respectively. Absolute ethanol was used as the solvent to dissolve UHMWPE and PTFE. Varied SiC papers were prepared, including 180#, 240#, 400#, 600#, 1000#, 1200#, and 1500#, for texturing the composite.

**Fig. 2** The surface morphologies of 10% PTFE under different levels of texture. **a** Without texture. **b–h** Textured by 180#, 240#, 400#, 600#, 1000#, 1200#, and 1500# SiC paper, respectively



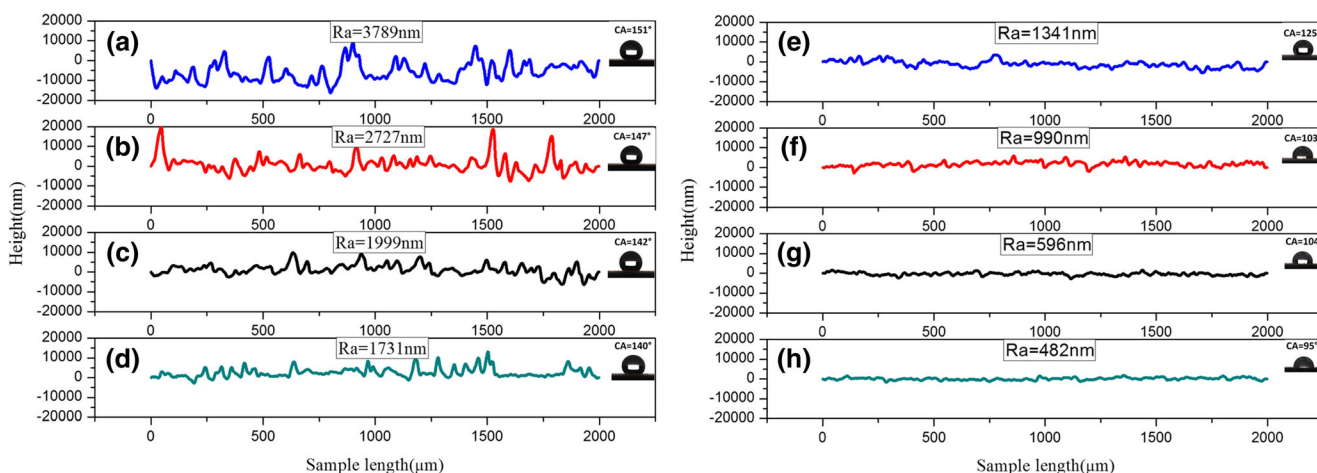


**Fig. 3** The roughness profile curves of 10% PTFE under different levels of texture. **a–g** Textured by 180#, 240#, 400#, 600#, 1000#, 1200#, and 1500# SiC paper respectively. **h** Without texture

### Fabrication of the superhydrophobic composite surface

PTFE nano-particles and UHMWPE powder were mixed (PTFE concentration is occupied for 0, 5, 8, 10, 12, 15%, respectively) and then ultrasonic oscillation for 30 min and stirring for 2 h in alcohol solution to dispersed uniformly. After that, the mixture was transferred to a 60 °C drier for 24 h for drying into powder. The drying powder mixture was added into the composite block by a hot-pressing process in the mold for 3–4 h under certain conditions of 200 °C with 2 MPa pressure. A 5 kg mass was loaded on the prepared sample, then we pushed the loaded sample on SiC sandpaper at a speed of 5 m/min, the sample push distance is 10 m, and the calculated contact pressure is 20 kPa between the sample and sandpaper. Finally, the superhydrophobic surface was fabricated successfully.

### Superhydrophobic surface characterization

The water contact angle (WCA) was measured using a surface tension instrument (JC2000D2A, China); each sample was measured with a 8- $\mu$ L deionized water drop at five different positions. The morphology of all the fabricated surfaces was observed using a scanning electronic microscope (SEM,

Quanta 250, FEI, America). A step profile (DektakXT, Bruker, Germany) was used to evaluate the surface roughness. Anti-icing performance was measured by humidity chamber whose temperature was turned to  $-20$  °C with a 90% relative humidity, and the samples were weighed before and after icing for 6 h. The water droplet bouncing movement was observed by a high-speed camera within 13  $\mu$ L at the height of 10 mm.

## Results and discussion

### Influence of different PTFE concentrations and texture morphology on the superhydrophobic surface properties

The PTFE/UHMWPE polymer were prepared with different PTFE concentrations of 0, 5, 8, 10, 12, and 15% and followed treatment by 180# SiC paper. Compared with the pure UHMWPE surface, the hydrophobic property of PTFE/UHMWPE surface was improved greatly; the contact angle increased from  $94^\circ$  to  $151^\circ$ . It was observed that the more of PTFE, the higher contact angle of the surface, which should be attributed to the increasing PTFE particles. However, when the PTFE concentration reached to 10%, the contact angle fluctuated at  $150^\circ$ ; this is due to that the excess PTFE powder

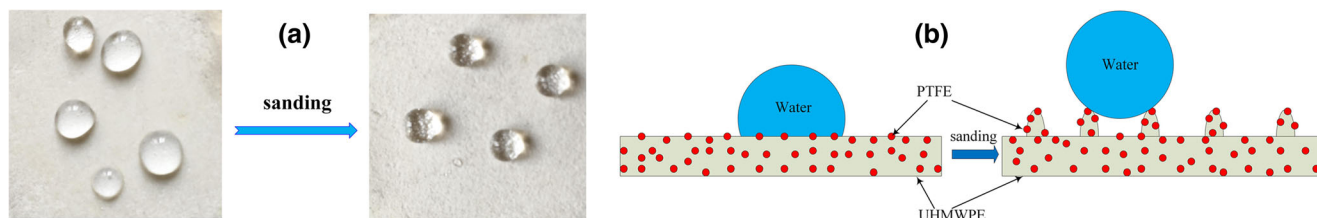
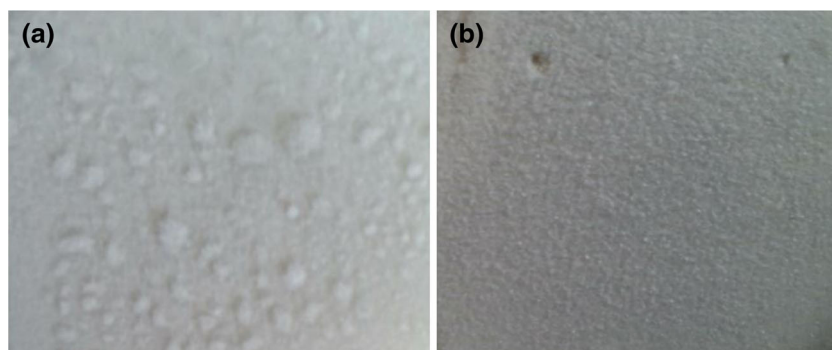


**Fig. 4** **a** Optical image of water droplets on the smooth and roughness surface. **b** Simplified model of the surface with microstructure smooth and roughness

**Fig. 5** Optical images of frost films after the steam freezing. **a** Smooth surface. **b** As-prepared superhydrophobic surface



distributed unevenly and generated aggregation (Fig. 1). Figure 2 shows the SEM images of 10% PTFE under different texture levels; the textured samples (Fig. 2b–h) possess a more rough structure compared with the surface without texturing (Fig. 2a). With the decrease of SiC paper roughness, the fibrous structure sizes became more and more finely. The contact angles of surface textured sample with 180# SiC paper and without texturing were  $151^\circ$  and  $95^\circ$ , respectively. Meanwhile, the corresponding surface roughness was measured and the  $R_a$  value was found to be 3789 and 482 nm in Fig. 3a, h. The  $R_a$  value was decreased from heavy-grade sandpaper to fine-grade sandpaper (Fig. 3). Figure 2b shows a surface with lots of high homogeneous plume protrusions due to the existence of larger SiC particles in 180# heavy-grade sandpaper. As the sandpaper grit increased to 240#, the contact angle decreased to  $147^\circ$ , and  $R_a$  value changes from 3789 to 2727 nm (Fig. 2c). The surface morphology of Fig. 2d, e is similar to Fig. 2c, but the  $R_a$  value decreases to 1999 and 1731 nm, and the corresponded contact angles were  $142^\circ$  and  $140^\circ$ , respectively. A remarkable change of surface morphology was observed in Fig. 2f: the surface became more uneven with fine fibrous structures with  $R_a$  value of 1341 nm and the contact angle decreased to  $125^\circ$  sharply. The apparent contact angle should exist in the Cassie state when water droplet contacted with the rough surface structure. In Fig. 2b–e, the plume structure with numerous space were filled with large amount of air and resulting in the larger contact angle. However, when the roughness of the textured surface

decreased, the water droplets would infiltrate into the substrate and the contact angle has a sharp decrease (Fig. 2f–h). Figure 2b shows an appropriate surface morphology, formed under a 180# SiC paper texturing, which obtained the best superhydrophobic properties.

#### The mechanism of the prepared superhydrophobic surface

The rough hierarchically micro-/nano-structures and the low surface energy of PTFE were very helpful for forming a cushion to store air and hold water droplet; the optical image is shown in Fig. 4a. The convex/concave structure was observed by scanning electron microscopy and it could be simplified into a model as shown in Fig. 4b. The micro-/nano-roughness and porosity can catch a lot of air and form an air cushion; as a result, the water cannot enter into the coating holes and voids, thus obtaining the superhydrophobic state. According to water droplets in the liquid, solid, and gas three-phase composite surface proposed by Cassie, the contact angle calculation formula can be expressed as follows [26]:

$$\cos\theta_c = f_1\cos\theta - f_2 \quad (1)$$

where  $\theta_c$  is the apparent contact angle of the rough surface,  $\theta$  is the apparent contact angle of the smooth surface,  $f_1$  is the percentage of droplets with a solid surface occupied by the composite interface, and  $f_2$  is the percentage of water droplets

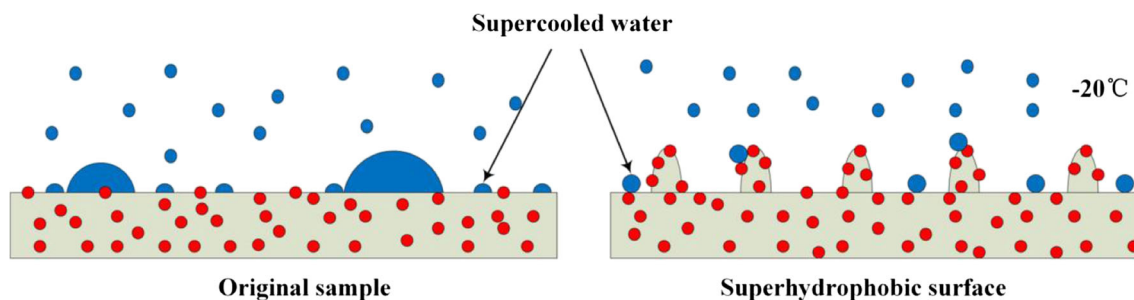


**Fig. 6** Simplified models of the steam freezing on smooth surface and superhydrophobic surface



**Fig. 7** Screenshots of dynamic contact process. **a** The smooth surface. **b** The superhydrophobic surface



in contact with the air interface ( $f_1 + f_2 = 1$ ). By measuring the smooth surface and the micro-/nano-composite surface, we can calculate the contact angle at  $95^\circ$  and  $150^\circ$ , respectively. It can be calculated that the  $f_2$  is 0.8532; obviously, the air in the proportion of the compound contact interface is as high as 85.32%.

### Anti-icing property

Figure 5 illustrated the results of the steam-freezing test of the smooth surface and the superhydrophobic surface, respectively. It can be easily found that there is a large ice film on the smooth surface while small ice film can be found on the superhydrophobic surface. The ice film covered the sample area 5 cm in diameter. The weight of the smooth sample varied from 21.5 to 21.7 g, and for the superhydrophobic sample, the mass varied from 22.4 to 22.5 g. That means the net-ice increment is 8.0 and 4.1  $\text{mg}/\text{cm}^2$  on the smooth and superhydrophobic surface, respectively, and the superhydrophobic surface can reduce almost half ice film compared with the smooth surface.

Figure 6 is a simplified model of the steam freezing on smooth surface and superhydrophobic surface in the environment of  $-20^\circ\text{C}$  and 90% relative humidity. Due to a small number of nucleation points on the smooth solid surface, the water vapor in the air forming supercooled water and contacting with the surface continues to increase, leading to larger ice film. Also, small ice crystals constantly grow and absorb the supercooled water bead from the air, resulting in

the larger amount of ice on the smooth surface. Meanwhile, the superhydrophobic surface possesses rough morphology and larger nucleation points. When supercooled water gets to the rough surface, it will form small and dense ice crystals immediately and cover the substrate on the superhydrophobic surface, which retards the absorption of supercooled water. In other words, the prepared superhydrophobic surface indicates an excellent anti-icing property.

### Low adhesion property analysis

The screenshots of dynamic contact angle are shown in Fig. 7. The water droplet only being  $4\ \mu\text{L}$ . The object stage was elevated slowly to make the sample surface contact with water droplet hanging on the needles. From Fig. 7a, we can see that the water droplet is stuck rapidly from the surface and gradually changes from sphere to triangulate on the compression and lifting process and finally has been caught on the surface, keeping Wenzel condition. As to the superhydrophobic surface, the water droplet changes from sphere to ellipsoid and finally remains sphere in the compression and lifting process, escaping easily from the surface, as is illustrated in Fig. 7b. In addition, the volume of the water droplet barely changes. In other words, the as-prepared superhydrophobic surface shows an excellent lower adhesive property.

In order to further characterize the sample surface adhesion force, we analyzed the droplet bouncing process, calculating the energy change of water droplet impacting the surface. Liu

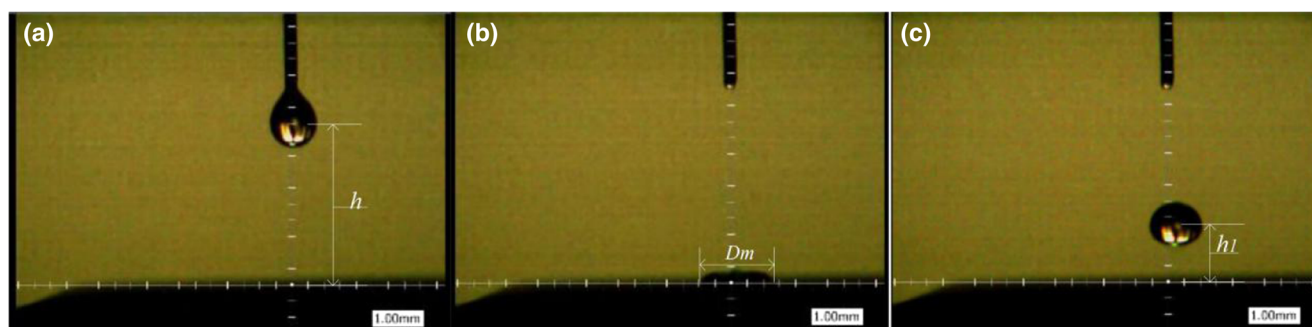


**Fig. 8** Screenshots of water droplet bouncing process. **a** The starting position. **b** Maximum diameter of spreading out. **c** Maximum height of bouncing

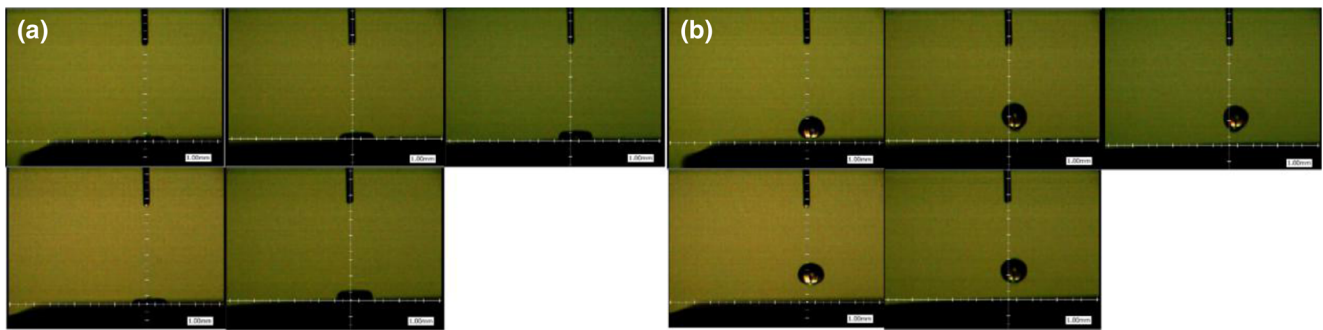


**Fig. 9** Screenshots of the first water droplet bouncing process. **a** Maximum diameter of spreading out. **b** Maximum height of bouncing

[27] characterized the loss of adhesion energy equaled to the energy of height difference between the starting position ( $h$ ) and maximum bounce height ( $h_1$ ), ignoring the change of surface energy and kinetic energy of the water droplet internal movement. Li [28] predicted the maximum diameter ( $D_m$ ) with building a model of spreading out. The surface energy of the largest diameter can be expressed as follows (Fig. 8b):

$$E_{s,1} = \frac{2}{3} \pi \sigma \frac{D_0^3}{D_m} + \frac{1}{4} \pi \sigma (1 - \cos \theta_c) D_m^2 \quad (2)$$

When getting to the top (Fig. 8c), water droplet's surface energy can be expressed as

$$E_{s,0} = \pi \sigma D_0^2 \quad (3)$$

and the gravitational potential energy as (Fig. 8c)

$$E_{k,2} = \frac{1}{6} \rho \pi g h_1 D_0^3 \quad (4)$$

where  $\sigma$  is the surface tension of water,  $D_0$  is water droplet diameter,  $\theta_c$  is the apparent contact angle, and  $\rho$  and  $g$  are the density of water and gravitational acceleration, respectively.

According to the conservation of energy, the surface energy of the largest diameter ( $E_{s,1}$ ) is converted into water droplet's surface energy of the top ( $E_{s,0}$ ), gravitational potential energy ( $E_{k,2}$ ), and kinetic energy of the water droplet internal movement ( $E_{k,1}$ ), which is expressed as

$$\begin{aligned} \frac{2}{3} \pi \sigma \frac{D_0^3}{D_m} + \frac{1}{4} \pi \sigma (1 - \cos \theta_c) D_m^2 \\ = \frac{1}{6} \pi \rho g h_1 D_0^3 + \pi \sigma D_0^2 + E_{k,1} \end{aligned} \quad (5)$$

We make the maximum spread factor ( $\beta$ ) represent the ratio of  $D_0$  and  $D_m$  and ignore  $E_{k,1}$  temporarily. The above is simplified as

$$8\sigma\beta^3 - (2\rho gh_1 D_0 + 12\sigma)\beta^2 + 3\sigma(1 - \cos \theta_c) = 0 \quad (6)$$

Only the maximum spread factor ( $\beta$ ) as the unknown, we can measure others to calculate that. In this experiment, the height of starting position ( $h$ ) is 10 mm and the water droplet diameter ( $D_0$ ) is 3 mm. In Fig. 9, five samples (PTFE concentrations 5, 8, 10, 12, 15%) were prepared with different contact angles ( $142^\circ$ ,  $145^\circ$ ,  $150^\circ$ ,  $149^\circ$ ,  $151^\circ$ ) and all the factors were measured in Table 1. The maximum spread factor ( $\beta_{11}$ ) can be calculated without the kinetic energy of the water droplet internal movement ( $E_{k,1}$ ) through Eq. 6. Compared with the experimental maximum spread factor ( $\beta_1$ ),  $\beta_{11}$  varies greatly. In other words, the existing  $E_{k,1}$  cannot be ignored, leading to the error experiment results. When the  $E_{k,1}$  was introduced to the equation, we can assume that the  $E_{k,1}$  is equal to  $E_{k,2}$ . Thus, the Eq. 6 can be redefined as

$$8\sigma\beta^3 - (4\rho gh_1 D_0 + 12\sigma)\beta^2 + 3\sigma(1 - \cos \theta_c) = 0 \quad (7)$$

Correctional maximum spread factor ( $\beta_{12}$ ) can be calculated from Eq. 7 in Table 1.

Figure 10 describes three situations of maximum spread factor on samples, including experimental, without  $E_{k,1}$ , and correctional. There is a large difference between the experimental maximum spread factor and without  $E_{k,1}$ . Meanwhile, the correctional maximum spread factor fits well with the experimental except the sample of 5% PTFE by  $E_{k,1}$

**Table 1** The samples factors of first water droplet bouncing process

PTFE content/%	Maximum spread diameter ( $D_m$ )/mm	Maximum bounce height ( $h_1$ )/mm	Experimental ( $\beta_1$ )	Without $E_{k,1}$ ( $\beta_{11}$ )	Correctional ( $\beta_{12}$ )
5	4.7	1.8	0.638	0.981	0.794
8	4.6	3.3	0.652	0.820	0.676
10	4.4	3.4	0.682	0.828	0.679
12	4.5	3.5	0.667	0.821	0.674
15	4.5	3.5	0.667	0.824	0.676

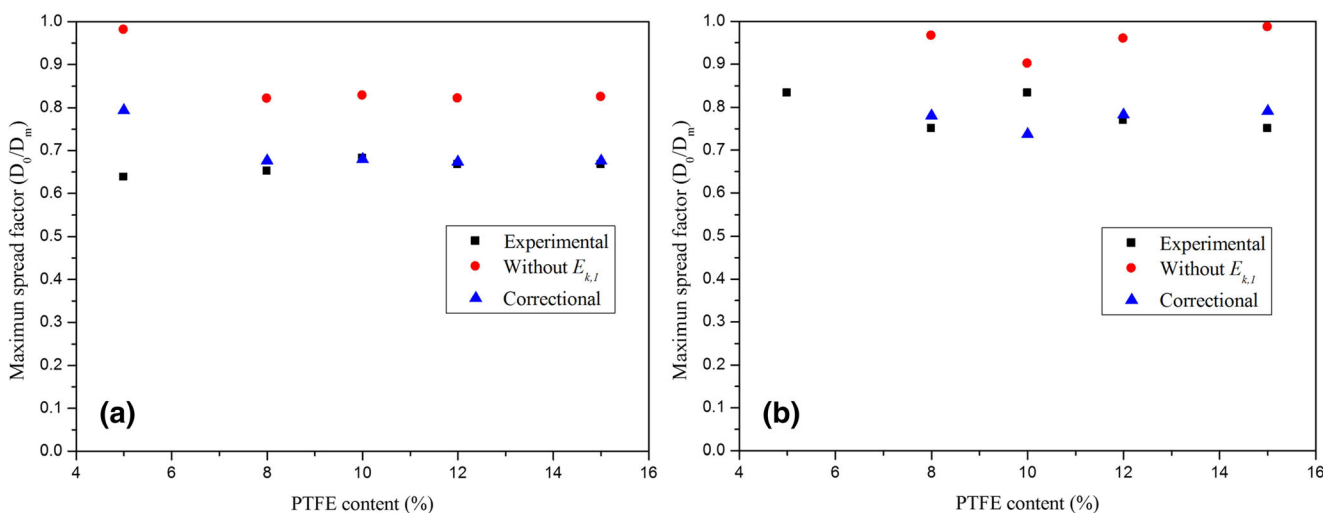


**Fig. 10** Maximum spread factor on samples. **a** First water droplet bouncing process. **b** Second water droplet bouncing process

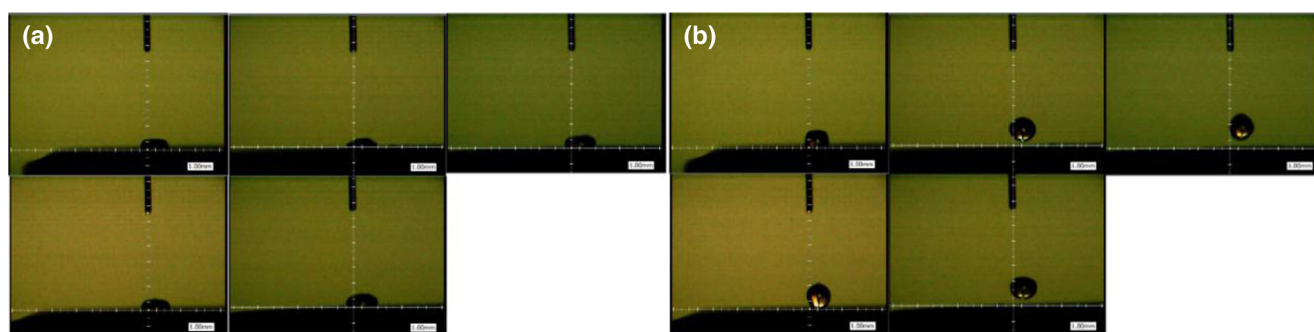


**Fig. 11** Screenshots of the second water droplet bouncing process. **a** Maximum diameter of spreading out. **b** Maximum height of bouncing

equivalent to  $E_{k,2}$  in Fig. 10a. Due to the sample of 5% PTFE has small contact angle, the droplet gets to the top, not divorced from the sample surface completely, leading to a large deviation of the correctional maximum spread factor.

In order to further verify the accuracy of the correctional maximum spread factor, we analyzed the second bounce process of water droplets in the same calculation (Fig. 11 and Table 2). Figure 10b portrays a same style of the correctional fitting the experimental. However, the solutions of Eqs. 6 and 7 (the factors sample of 5% PTFE) do not exist. The reason is that the droplet has not enough height of a bouncing and been caught by solid surface. In this condition, the  $E_{k,1}$  and  $E_{k,2}$  have great disparity compared with other samples, which cannot be applied to Eqs. 6 and 7.

According to the above experiment, the assumption of  $E_{k,l}$  being equal to  $E_{k,2}$  is relatively accurate in the superhydrophobic surface. We can solve the off-energy of contacting between the water droplet and superhydrophobic surface ( $E_w$ ), which can be expressed as

$$E_w = E_{k,0} - E_{k,1} - E_{k,2} \tag{8}$$

where  $E_{k,0}$  is the starting gravitational potential energy.  $E_w$  can be calculated as a characterization of low adhesion property. The off-energy of contacting between water droplets and superhydrophobic surface accounts for approximately 30% of the starting gravitational potential energy.

**Table 2** The samples factors of second water droplet bouncing process

PTFE content/%	Maximum spread diameter ( $D_{m1}$ )/mm	Maximum bounce height ( $h_1$ )/mm	Experimental ( $\beta_1$ )	Without $E_{k,1}$ ( $\beta_{11}$ )	Correctional ( $\beta_{12}$ )
5	3.6	0.6	0.833	None	None
8	4.0	2.1	0.750	0.966	0.780
10	3.6	2.6	0.833	0.901	0.737
12	3.9	1.9	0.769	0.959	0.782
15	4.0	2.0	0.750	0.986	0.791

## Conclusion

In summary, we have developed a simple, rapid, and energy-saving approach to fabricate PTFE/UHMWPE superhydrophobic surface, which is suitable for large-scale manufacturing and has a good potential application prospect. We analyzed the main factors affecting the superhydrophobicity and reached some conclusions as follows: as the PTFE concentration is 10% and the sandpaper is 180#, the optimal superhydrophobic surface is prepared with a contact angle of 151°. The as-prepared surface has been demonstrated that it has excellent anti-icing performance and low adhesive property. Meanwhile, the off-energy can be calculated as a characterization of low adhesion property, which accounts for approximately 30% of the initial gravitational potential energy at a 10 mm height.

**Acknowledgement** This work was supported by the National Nature Science Foundation of China (No.51475457) and Qing Lan Project. We express our grateful thanks to them for their financial support.

## Compliance with ethical standards

**Conflict of interest** The authors declare that they have no conflict of interest.

## References

- Wang S, Jiang L (2007) Definition of superhydrophobic states. *Adv Mater* 19(21):3423–3424
- Sas I, Gorga RE, Joines JA, et al (2012) Literature review on superhydrophobic self-cleaning surfaces produced by electrospinning. *Journal of Polymer Science Part B Polymer Physics* 50(12):824–845
- Jiang YD, Kitada M, White M, et al (2014) Development of durable nanostructured superhydrophobic self-cleaning surfaces on glass substrates. *J Food Process Preserv* 38(3):1321–1329
- Xiu Y, Hess DW, Wong CP (2008) UV-resistant and superhydrophobic self-cleaning surfaces using sol–gel processes. *Journal of Adhesion Science & Technology* 22(15):1907–1917
- Xu QF, Wang JN, Smith IH, et al (2009) Superhydrophobic and transparent coatings based on removable polymeric spheres. *J Mater Chem* 19(5):655–660
- Xu L, He J (2012) Fabrication of highly transparent superhydrophobic coatings from hollow silica nanoparticles. *Langmuir* 28(19):7512–7518
- Cao L, Gao D (2010) Transparent superhydrophobic and highly oleophobic coatings. *Faraday Discuss* 146(1):57–65
- Sun Z, Liao T, Liu K, et al (2014) Superhydrophobic materials: fly-eye inspired superhydrophobic anti-fogging inorganic nanostructures (small 15/2014). *Small* 10(15):3001–3006
- Kidin IN, Shcherbedinskii GV, Andryushechkin VI, et al (2013) Mg alloy treatment for superhydrophobic anticorrosion coating formation. *Surface Innovations* 1(3):162–172
- Li J, Zhao Z, Zhang Y, et al. Facile fabrication of superhydrophobic silica coatings with excellent corrosion resistance and liquid marbles. *Journal of Sol-Gel Science and Technology*, 2016.
- She Z, Li Q, Wang Z, et al (2013) Researching the fabrication of anticorrosion superhydrophobic surface on magnesium alloy and its mechanical stability and durability. *Chem Eng J* 228(28):415–424
- Li J, Shi L, Chen Y, et al (2012) Stable superhydrophobic coatings from thiol-ligand nanocrystals and their application in oil/water separation. *J Mater Chem* 22(19):9774–9781
- Lei W, Zhang J, Li B, et al (2014) Mechanical- and oil-durable superhydrophobic polyester materials for selective oil absorption and oil/water separation. *Journal of Colloid & Interface Science* 413(1):112–117
- Cao L, Jones AK, Sikka VK, et al (2009) Anti-icing superhydrophobic coatings. *Langmuir the ACS Journal of Surfaces & Colloids* 25(21):12444–12448
- Wang F, Yu S, Ou J, et al (2015) Anti-icing performance of transparent and superhydrophobic surface under wind action. *J Sol-Gel Sci Technol* 75(3):625–634
- Cheng Z, Du M, Lai H, et al (2013) Selective transportation of microdroplets assisted by a superhydrophobic surface with pH-responsive adhesion. *Chem Asian J* 8(12):3200–3206
- Ishii D, Yabu H, Shimomura M (2010) Micro droplet transfer between superhydrophobic surfaces via a high adhesive superhydrophobic surface. In: *Biomedical engineering systems and technologies*. Springer, Berlin, pp. 136–142
- Li J, Jing Z, Zha F, et al (2014) Facile spray-coating process for the fabrication of tunable adhesive superhydrophobic surfaces with heterogeneous chemical compositions used for selective transportation of microdroplets with different volumes. *ACS Appl Mater Interfaces* 6(11):8868–8877
- Zhang X, Shi F, Niu J, et al (2008) Superhydrophobic surfaces: from structural control to functional application. *J Mater Chem* 18(6):621–633
- Bhushan B, Yong CJ (2011) Natural and biomimetic artificial surfaces for superhydrophobicity, self-cleaning, low adhesion, and drag reduction. *Prog Mater Sci* 56(1):1–108
- Song H J, Zhang Z Z, Men X H. Superhydrophobic PEEK/PTFE composite coating. *Proceedings of 5th International Symposium on High-Tech Polymer Materials*. 2008:73–76.
- Cardoso MR, Tribuzi V, Balogh DT, et al (2011) Laser microstructuring for fabricating superhydrophobic polymeric surfaces. *Appl Surf Sci* 257(8):3281–3284
- Huang Y, Hu Y, Zhu C, et al. Long-lived multifunctional superhydrophobic heterostructure via molecular self-supply. *APS Meeting*. APS Meeting Abstracts, 2016.
- Oral E, Neils AL, Wannomae KK, et al (2014) Novel active stabilization technology in highly crosslinked UHMWPEs for superior stability. *Radiation Physics & Chemistry* 105:6–11
- Chen Y, Li Y, Zou H, et al (2014) Effect of solid-state shear milling on structure and properties of HDPE/UHMWPE blends. *J Appl Polym Sci* 131(4):1001–1007
- Cassie ABD, Baxter S (1944) Wettability of porous surfaces. *Trans Faraday Soc* 40:546–551
- Chen T, Ge S, Liu H, et al (2015) Fabrication of low adhesive superhydrophobic surfaces using nano Cu/Al<sub>2</sub>O<sub>3</sub> Ni-Cr composited electro-brush plating. *Appl Surf Sci* 356:81–90
- Xiying L, Xuehu M, Zhong L (2010) Dynamic behavior of the water droplet impact on a textured hydrophobic/superhydrophobic surface: the effect of the remaining liquid film arising on the pillars' tops on the contact time. *Langmuir* 26(26):4831–4838